

Electronic Structure and Electron-Phonon Interaction in Hexagonal Yttrium

Prabhakar P. Singh*

Department of Physics, Indian Institute of Technology, Powai, Mumbai- 400076, India

To understand the pressure-induced changes in the electronic structure and the electron-phonon interaction in yttrium, we have studied hexagonal close-packed (hcp) yttrium, stable at ambient pressure and double hexagonal close-packed (dhcp) yttrium, stable up to around 44 GPa, using density-functional-based methods. Our results show that as one goes from hcp yttrium to dhcp yttrium, there is (i) a substantial charge-transfer from $s \rightarrow d$ with extensive modifications of the d -band and a sizable reduction in the density of states at the Fermi energy, (ii) a substantial stiffening of phonon modes with the electron-phonon coupling covering the entire frequency range, (iii) an increase in the electron-phonon coupling constant λ from 0.55 to 1.24, leading to a change in the superconducting transition temperature T_c from 0.3 K to 15.3 K for $\mu^* = 0.2$.

I. INTRODUCTION

The change in the superconducting transition temperature T_c in yttrium from 6 mK at ambient pressure¹ to around 20 K at 115 GPa², concurrent with the change in its crystal structure^{3,4}, underscores the intricate relationship between pressure-induced $s \rightarrow d$ charge transfer, dynamical response of the lattice and its coupling to Fermi electrons. The experiment on yttrium follows the recent observation of superconductivity in compressed lithium at a T_c of 20 K^{5,6}, bringing into focus the pressure-induced changes in the electron-phonon interactions in elemental metals, especially the alkali and the early-transition metals^{7,8,9}.

Experimentally, yttrium follows the equilibrium structure sequence hcp \rightarrow Sm-type \rightarrow dhcp \rightarrow trigonal as the pressure is increased from ambient to 50 GPa at room temperature³. It is expected that yttrium will stabilize in a body-centered cubic structure at pressures above 280 GPa¹⁰. On the other hand, The superconducting transition temperature T_c changes from 6 mK at ambient pressure¹ to around 1.3 K at 11 GPa¹¹, and then to 17 K at 89 GPa². A further increase in pressure to 115 GPa results in a $T_c = 20$ K. Surprisingly, it seems possible that for pressures greater than 115 GPa, yttrium could superconduct with a T_c higher than that of 20 K.

In an effort to understand the pressure-induced changes in the superconducting properties of yttrium *vis-a-vis* the changes in its stable crystal structure, we have studied, using density-functional based methods, (i) the electronic structure, (ii) the phonon density of states, (iii) the electron-phonon interaction, and (iv) the solutions of the isotropic Eliashberg gap equation for hcp and dhcp yttrium at ambient pressure and at around 50 GPa.

We have calculated the electronic structure of hcp and dhcp yttrium using full-potential, linear muffin-tin orbital (LMTO) method^{12,13} as well as the plane-wave pseudopotential method using Quantum-ESPRESSO package¹⁴. Using the linear response code based on the LMTO method, we have calculated the phonon DOS, $F(\omega)$, and the Eliashberg function, $\alpha^2 F(\omega)$, for hcp and dhcp yttrium. Subsequently, we have numerically solved the isotropic Eliashberg gap equation^{15,16,17} for a range

of μ^* to obtain the corresponding superconducting transition temperature T_c . After the completion of the present work, we have come across the work of Yin *et al.*¹⁸, which uses the *hypothetical* fcc structure to describe the effects of pressure in yttrium.

Based on our calculations, described below, we find that as one goes from hcp yttrium to dhcp yttrium, there is (i) a substantial charge-transfer from $s \rightarrow d$ with extensive modifications of the d -band, (ii) a stiffening of phonon modes with the electron-phonon coupling over the entire frequency range, (iii) an increase in electron-phonon coupling constant λ from 0.55 to 1.24, leading to a change in the superconducting transition temperature T_c from 0.3 K to 15.3 K for $\mu^* = 0.2$, consistent with experiment.

II. THEORETICAL APPROACH AND COMPUTATIONAL DETAILS

The density-functional theory provides a reliable framework for implementing from first-principles the Migdal-Eliashberg approach for calculating the superconducting properties of metals. Such an approach has been implemented using the full-potential LMTO method^{12,13}.

In general, the phonon density of states is given by

$$F(\omega) = \sum_{\mathbf{q}\nu} \delta(\omega - \omega_{\mathbf{q}\nu}),$$

where $\omega_{\mathbf{q}\nu}$ is the $q\nu$ -th phonon mode associated with the atomic displacements. Using the electron-phonon matrix elements $g_{\mathbf{k}+\mathbf{q}j',\mathbf{k}j}^{\mathbf{q}\nu}$, which can be interpreted as the scattering of electron in state $|\mathbf{k}j\rangle$ to state $|\mathbf{k}+\mathbf{q}j'\rangle$ due to perturbation arising out of the phonon mode $\omega_{\mathbf{q}\nu}$, we can calculate the phonon line width $\gamma_{\mathbf{q}\nu}$

$$\gamma_{\mathbf{q}\nu} = 2\pi\omega_{\mathbf{q}\nu} \sum_{\mathbf{k}jj'} |g_{\mathbf{k}+\mathbf{q}j',\mathbf{k}j}^{\mathbf{q}\nu}|^2 \delta(\epsilon_{\mathbf{k}j} - \epsilon_F) \delta(\epsilon_{\mathbf{k}+\mathbf{q}j'} - \epsilon_F).$$

where $N(\epsilon_F)$ is the electronic density of states at the Fermi energy. Now, we can combine the electronic density of states, phonon spectrum and the electron-phonon matrix elements to obtain the Eliashberg function $\alpha^2 F(\omega)$ defined as

$$\alpha^2 F(\omega) = \frac{1}{2\pi N(\epsilon_F)} \sum_{\mathbf{q}\nu} \frac{\gamma_{\mathbf{q}\nu}}{\omega_{\mathbf{q}\nu}} \delta(\omega - \omega_{\mathbf{q}\nu})$$

Finally, the Eliashberg functions can be used to solve the isotropic gap equation^{15,16,17}

$$\Delta(i\omega_n) = \sum_{n'}^{| \omega_{n'} | < \omega_c} f_{n'} S(n, n') \Delta(i\omega_{n'})$$

to obtain the superconducting properties such as the superconducting transition temperature T_c . The function $S(n, n')$ used in the gap equation is defined by

$$S(n, n') \equiv \lambda(n - n') - \mu^* - \delta_{nn'} \sum_{n''} s_n s_{n''} \lambda(n - n'')$$

and $f_n = 1/|2n + 1|$ with s_n representing the sign of ω_n . The electron-phonon coupling $\lambda(\nu)$ is given by

$$\lambda(\nu) = \int_0^\infty d\omega \alpha^2 F(\omega) \frac{2\omega}{\omega_\nu^2 + \omega^2}.$$

Before describing our results, we provide some of the computational details of the present calculations.

The self-consistent electronic structures of hcp and dhcp yttrium in $P6_3/mmc$ crystal structure, having two and four yttrium atoms in the respective primitive cells, were calculated using the pwscf code of the Quantum-ESPRESSO package and the full-potential, LMTO method. The results obtained with the pwscf code are used to study the equation of state of yttrium. All other properties of yttrium, described below, have been obtained with the full-potential, LMTO method and linear response code based on the LMTO method.

The plane-wave pseudopotential method with Vanderbilt's ultrasoft pseudopotentials were used to calculate the electronic structure of hcp and dhcp yttrium with 259 \mathbf{k} -points in the irreducible Brillouin zones. The ultrasoft pseudopotential used also included the 4s and 4p states with nonlinear core correction. The kinetic energy cutoff for the wavefunction was taken to be 35 Ry, while for the charge density and the potential the kinetic energy cutoff were 200 Ry. For exchange-correlation potential we used the local-density approximation as given by Perdew *et al*¹⁹. These calculations were used to study the equation of state of yttrium.

The charge self-consistent, full-potential, linear muffin-tin orbital calculations for hcp and dhcp yttrium were carried out with the local-density approximation for exchange-correlation of Perdew *et al*¹⁹ with 2κ -energy panels and 610 and 549 \mathbf{k} -points respectively, in the corresponding irreducible wedges of the hexagonal Brillouin zones. The 4s state of yttrium was treated as a semicore state, while the 4p state was treated as a valence state. The basis set used consisted of s , p , and d orbitals at the yttrium site, and the potential and the wave function were expanded up to $l_{max} = 6$. The muffin-tin radii for

yttrium at zero pressure and at 50 GPa were taken to be 3.3 and 2.8 atomic units, respectively. These calculations were used to study the s -, p - and d -resolved densities of states, the band-structure along the high symmetry directions in the hexagonal Brillouin zones and the Fermi surfaces of hcp and dhcp yttrium. The Fermi surfaces of hcp and dhcp yttrium were constructed using XCrySDen program²⁰ with eigenvalues calculated on a $36 \times 36 \times 24$ and $36 \times 36 \times 12$ grid in the reciprocal space respectively.

The phonon density of states and the Eliashberg function of hcp and dhcp yttrium were calculated using the linear response code based on the full-potential, LMTO method. The dynamical matrices and the electron-phonon matrix elements of hcp and dhcp yttrium were calculated on a $6 \times 6 \times 4$ and $6 \times 6 \times 2$ grids respectively, resulting in 21 and 14 irreducible \mathbf{q} -points. The Brillouin zone integrations during linear response calculations for hcp and dhcp yttrium were carried out using a $12 \times 12 \times 8$ and $12 \times 12 \times 4$ grids of \mathbf{k} -points. The Fermi surface sampling for the evaluation of the electron-phonon matrix elements for the two structures were done using $36 \times 36 \times 24$ and $36 \times 36 \times 12$ grids.

III. RESULTS AND DISCUSSION

In this section we describe the results of our calculations of the electronic structure, the linear response and the solutions of the isotropic Eliashberg gap equation for hcp and dhcp yttrium. Our results are described in terms of (i) equation of state, (ii) electronic structure, (iii) electron-phonon interaction, and (iv) superconducting transition temperature obtained from the solutions of the isotropic Eliashberg gap equation.

A. Equation of State

The calculated equations of state of yttrium in hcp and dhcp phases are shown in Fig. 1. These equations of state are obtained by fitting the calculated total energy versus volume points to the third-order Birch-Murnaghan equation of state²¹. The value of c/a was optimized by iteratively minimizing the total energy as a function of volume. The lattice constants a and c at zero and 50 GPa for both hcp and dhcp phases, as obtained through the above procedure, are given in Table I. However, the lattice constant a for the high-pressure dhcp phase of yttrium corresponds to the compressed volume equal to $0.56v_0$, with the ideal $c/a = 3.25$ and where v_0 is the experimentally determined equilibrium volume of the hcp phase. The lattice constants as given in Table I have been used in all the calculations reported below. We also note that in our discussion, we will emphasize the stable structures, viz. hcp at zero pressure and dhcp at 50 GPa pressure, more than the unstable structures at these pressures.

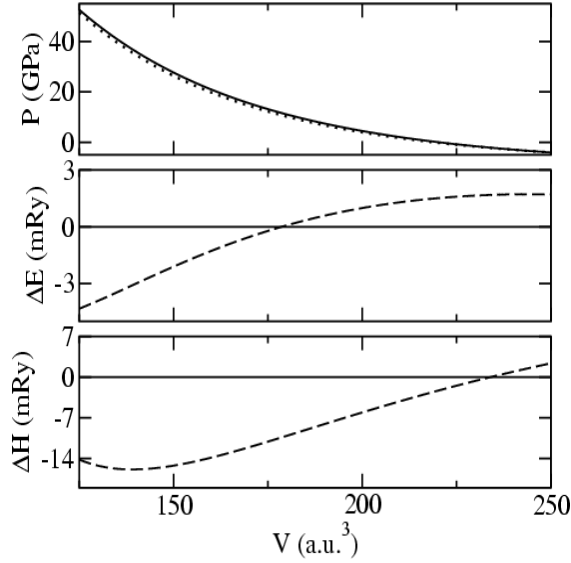


Figure 1: The equation of state (top panel) of hcp (solid line) and dhcp (dotted line) yttrium, the difference in energy ΔE (middle panel, dashed line) and enthalpy ΔH (bottom panel, dashed line) of dhcp yttrium with respect to hcp yttrium as a function of volume per atom.

Table I: The lattice constants of hcp and dhcp yttrium used in the calculations. The experimental values³ are given in the parentheses.

structure	pressure (GPa)	a (a.u.)	c/a
hcp	0	6.775 (6.895)	1.56 (1.571)
hcp	50	5.604	1.65
dhcp	0	6.811	3.20
dhcp	50	5.619	3.25

The calculated lattice constants for hcp yttrium at zero pressure, as given in Table I, are somewhat smaller than the experimental values, as expected in local-density approximation. We find the bulk modulus of hcp yttrium at equilibrium to be 39.4 GPa, which compares well with the experimental value of 41 GPa³. In Fig. 1, we also show the energy and enthalpy of dhcp yttrium with respect to hcp yttrium as a function of volume. At zero pressure the dhcp phase is approximately 3 mRy higher in energy than the hcp phase. However, with increase in pressure both energy and enthalpy of the dhcp phase becomes lower than the hcp phase, in agreement with experiment.

B. Electronic Structure

We show in Fig. 2, the calculated band-structure along high symmetry directions in the hexagonal Brillouin zones of hcp and dhcp yttrium at both zero and at 50 GPa pressure. The band corresponding to $4p$ state is much lower in energy, and it is not shown in the figure.

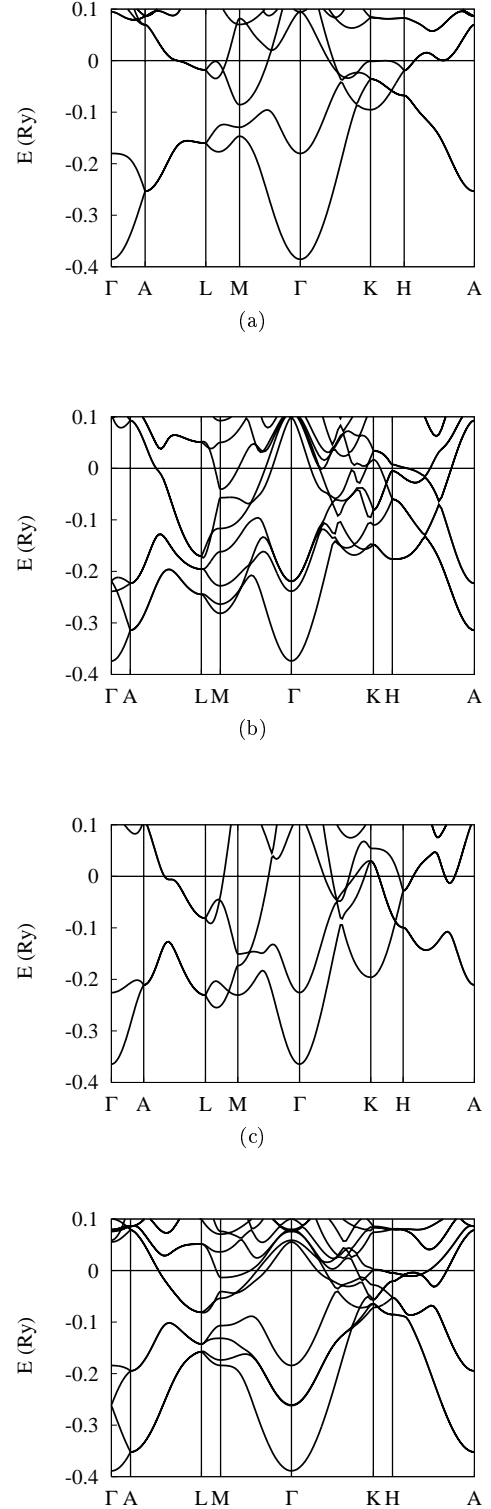


Figure 2: The band-structure along high symmetry directions in the hexagonal Brillouin zones of (a) hcp yttrium at ambient pressure, (b) dhcp yttrium at 50 GPa, (c) hcp yttrium at 50 GPa and (d) dhcp yttrium at ambient pressure. The horizontal line, passing through the energy zero, indicates the Fermi energy.

We find that in the case of hcp yttrium at zero pressure only two bands, the 3rd and the 4th bands in Fig. 2 (a), cross the Fermi energy. Based on the band-structure, we expect the states close to the zone boundary such as M, K, H, and L symmetry points to contribute to the electron-phonon coupling. For dhcp yttrium with 4-atom basis, we find that there are four bands crossing the Fermi energy at 50 GPa, as shown in Fig. 2 (b). There are states around symmetry points M, K and H that are close to Fermi energy, therefore we expect these states to play an important role in electron-phonon coupling in compressed dhcp yttrium. Due to charge transfer from $s \rightarrow d$ the bottom of the s -band moves slightly up in dhcp yttrium as can be seen by comparing Figs. 2 (a) and 2 (b).

In Figs. 2 (c)-(d), we show the band-structure of hcp phase at high pressure and dhcp phase at ambient pressure, respectively. We find that the increase in pressure has changed the band-structure of the hcp phase, especially along Γ -A and around symmetry points K and H, in such a way that it looks similar to the high pressure dhcp phase. In particular, the flat portion along K-H in the hcp phase, as shown in Fig. 2 (a), has been completely modified at high pressure, as shown in Fig. 2 (c).

A more comprehensive picture of $s \rightarrow d$ charge transfer can be obtained by comparing the densities of states of hcp and dhcp yttrium. In Fig. 3, we show the total and the l -resolved densities of states of hcp and dhcp yttrium. By comparing the total densities of states in the two structures, we find that many more states are created between -0.26 Ry and -0.16 Ry in the compressed dhcp yttrium to accommodate the pushed out s -electrons as well as the d -electrons pushed further inside from the flattened portion of the d -band near the Fermi energy. We also find that in the energy interval -0.2 Ry to -0.05 Ry, some p -states are also created in the compressed dhcp yttrium.

The density of states around the Fermi energy plays an important role in determining the electron-phonon interaction in metals. In the present case, we find that the total density of states of 22.8 st/Ry atom at the Fermi energy in hcp yttrium reduces to 13.4 st/Ry atom in dhcp yttrium. The reduction in s and d states are from 0.71 and 20.9 st/Ry atom in hcp yttrium to 0.6 and 11.7 st/Ry atom in dhcp yttrium, respectively. Usually, an increase in the density of states at the Fermi energy strengthens the electron-phonon coupling. However, in spite of a decrease in the density of states at the Fermi energy as yttrium is compressed, there is an increase in the strength of the electron-phonon coupling.

The changes in the densities of states of the unstable phases of yttrium, namely hcp at high pressure and dhcp at ambient pressure, are shown in Fig. 3 (b). The pressure-induced changes in going from ambient pressure dhcp phase to high pressure hcp phase are qualitatively similar to that of hcp to dhcp as described above. For example, the total density of states of 21.1 st/Ry atom at the Fermi energy in dhcp yttrium, at ambient pressure,

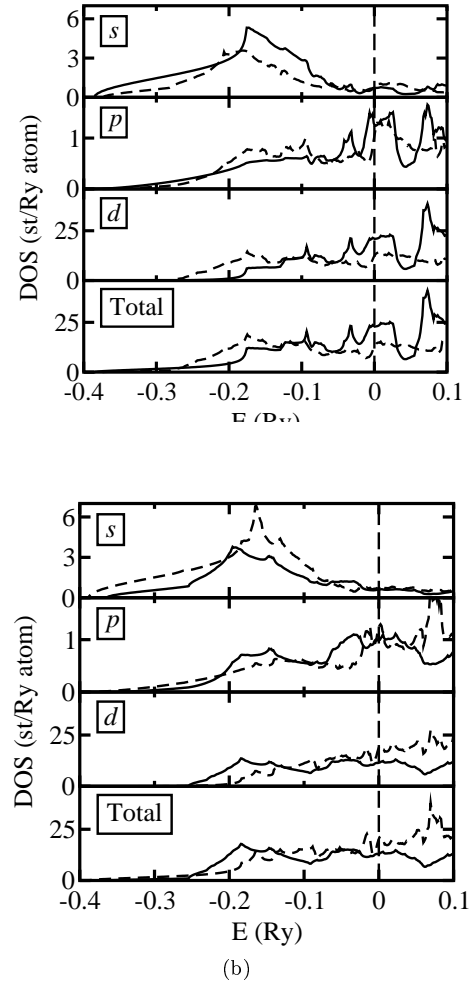


Figure 3: The s , p , d and the total densities of states of (a) hcp yttrium at ambient pressure (solid line) and dhcp yttrium at 50 GPa (dashed line), and (b) hcp yttrium at 50 GPa (solid line) and dhcp yttrium at ambient pressure (dashed line). The vertical, dashed line indicates the Fermi energy.

reduces to 13.1 st/Ry atom in hcp yttrium at high pressure. The changes in s and d states are from 0.58 and 19.3 st/Ry atom in dhcp yttrium to 0.6 and 11.5 st/Ry atom in hcp yttrium at high pressure, respectively.

The topology of the Fermi surface is useful in understanding many of the reciprocal-space-based properties of the solids. In particular, flat portions of the Fermi surface can give rise to peaks in the response function, leading to a substantial increase in the response function. In the case of compressed lithium, it has been shown that the flat portions of the corresponding Fermi surface, resulting in Fermi surface nesting, substantially enhance the electron-phonon interaction^{7,8,9}.

In the present case, the calculated Fermi surfaces of hcp and dhcp yttrium are shown in Fig. 4. In hcp yttrium, the 3rd band gives rise to a cylindrical tube along Γ -A, connected to a pancake-like structure with hexagonal symmetry on either end, while the fourth band gives

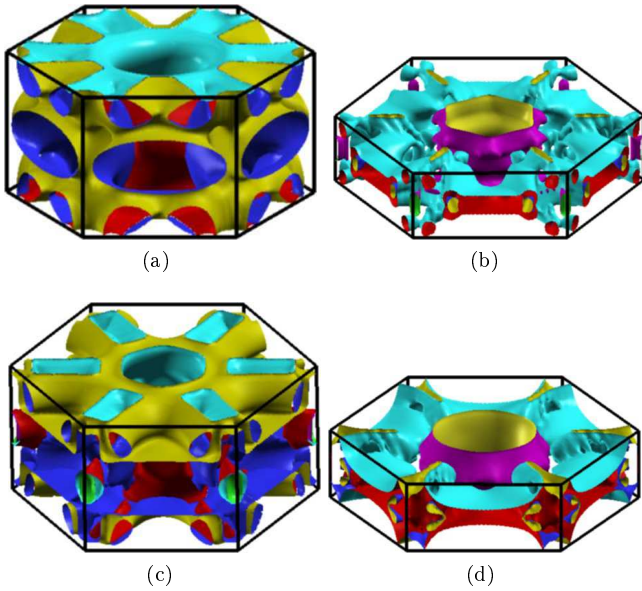


Figure 4: The Fermi surface of (a) hcp yttrium at ambient pressure, (b) dhcp yttrium at 50 GPa, (c) hcp yttrium at 50 GPa, and (d) dhcp yttrium at ambient pressure.

rise to a cylindrical tube along Γ -A with a bigger radius. Due to pressure, the Fermi surface of yttrium is substantially altered, as can be seen in Fig. 4 where we also show the Fermi surface of dhcp yttrium. The most obvious thing to note is the reduction along k_z -direction of the Fermi surface of dhcp yttrium by half. It is due to the doubling of the unit cell along the z -direction as one goes from hcp to dhcp structure. The cylindrical tube has separated from the pancake-like surface and, in addition, we find some flat portions on the M-K-H-L plane with *webbing*²² like features.

As shown in Figs. 4 (c)-(d), the change in pressure does not substantially alter the shape of the Fermi surfaces of either hcp or dhcp phase. However, to be able to compare the Fermi surfaces of hcp and dhcp phases at ambient pressure, we have calculated the Fermi surface of hcp phase after doubling the length of its primitive cell along c -direction. A band-by-band comparison of the two Fermi surfaces of hcp and dhcp phases at ambient pressure is shown in Fig. 5. The smaller values of a and c/a in hcp phase compared to dhcp phase are responsible for bigger Brillouin zones corresponding to the hcp phase. The differences in the Fermi surfaces of the two phases can then be attributed to the way the four basis atoms are distributed in the respective unit cells.

C. Electron-Phonon Interaction

The primary objective of the present study is to understand the pressure-induced increase in the superconducting transition temperature T_c of yttrium. Within the conventional BCS theory of superconductivity, a

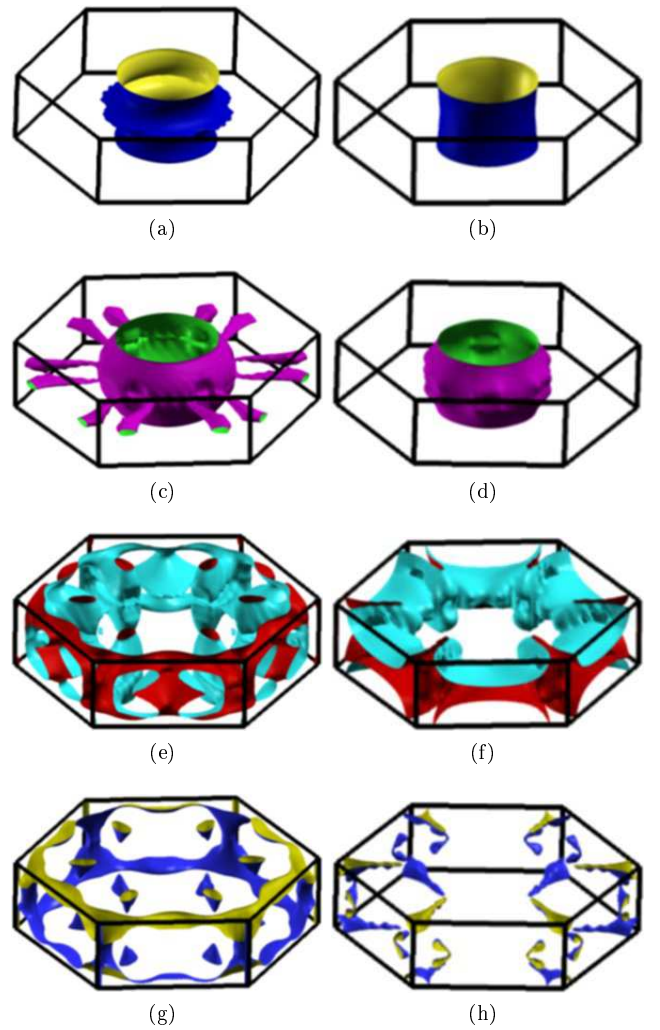


Figure 5: The Fermi surface of hcp (left column) and dhcp (right column) yttrium, both at ambient pressure, corresponding to (a-b) band number 1, (c-d) band number 2, (e-f) band number 3, and (g-h) band number 4.

change in T_c arises due to changes in the phonon spectrum and/or the electron-phonon spectral function (also known as the Eliashberg function). Usually, with increasing pressure the lattice hardens resulting in an increase in the phonon frequencies. At the same time, it is also possible for some phonon modes to soften and, in some cases, it may lead to lattice instability.

In Fig. 6, we show the phonon density of states $F(\omega)$ of stable hcp and dhcp yttrium, calculated using the density-functional theory as described earlier. The phonon density of states of hcp yttrium, as given in Fig. 6, is somewhat harder than the results of Heid *et al*²³. The maximum phonon frequency is about 29 meV with a large peak centered at 26 meV. We find that for $\mathbf{q} = \mathbf{0}$, the maximum frequency has a contribution from the two basis atoms moving along the z -axis in opposite directions. By comparing the $F(\omega)$ of dhcp yttrium with that of stable hcp phase, we clearly see the hardening of the

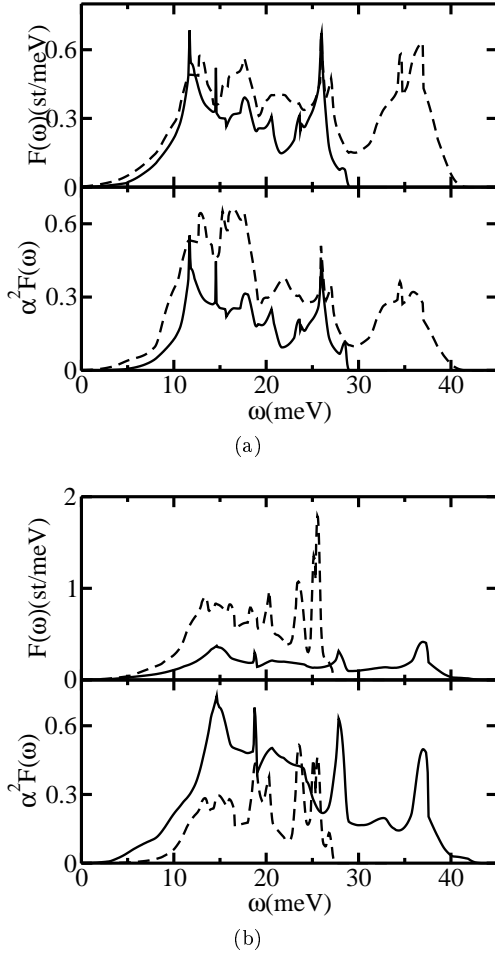


Figure 6: The phonon density of states $F(\omega)$ (top panels in (a) and (b)) and the Eliashberg function $\alpha^2 F(\omega)$ (bottom panels in (a) and (b)) of (a) hcp yttrium at ambient pressure (solid line) and dhcp yttrium at 50 GPa (dashed line), and (b) hcp yttrium at 50 GPa (solid line) and dhcp yttrium at ambient pressure (dashed line).

lattice as reflected in the increase of the maximum frequency to 41.8 meV with a broad peak at around 36.9 meV. We find that for $\mathbf{q} = \mathbf{0}$, the maximum frequency has contribution from the four basis atoms, separated into two groups of equivalent atoms, both groups moving along the z -axis in opposite directions.

To see the pressure-induced changes in the electron-phonon interaction in yttrium, we have calculated the Eliashberg function $\alpha^2 F(\omega)$ of hcp and dhcp yttrium as shown in Fig. 6. A comparison of $\alpha^2 F(\omega)$ of hcp and dhcp yttrium shows that the electron-phonon coupling is weaker in hcp yttrium than in dhcp yttrium. In particular, the average electron-phonon coupling constant λ is equal to 0.55 for hcp yttrium and 1.24 for dhcp yttrium. The pressure-induced increase in λ occurs due to enhanced coupling between 12 – 25 meV and due to the coupling of those phonons that arise due to the hardening of the lattice. Thus, we find that the Eliashberg

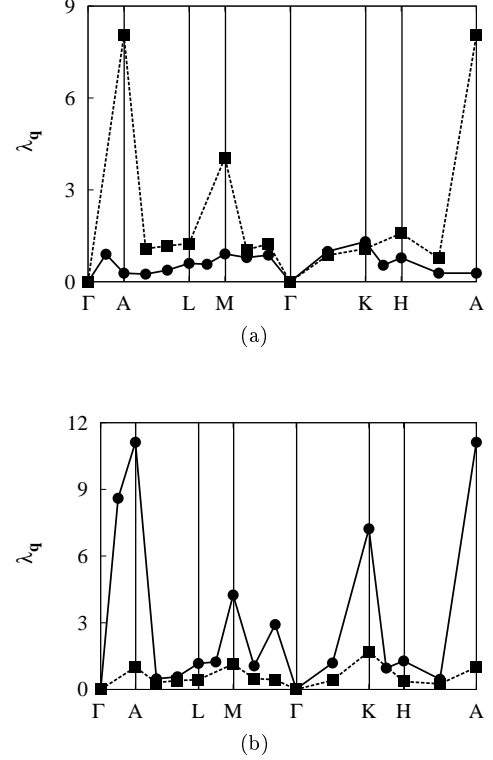


Figure 7: The partial $\lambda_{\mathbf{q}}$ along high symmetry directions in the hexagonal Brillouin zones of (a) hcp yttrium at ambient pressure (filled circles connected with solid line) and dhcp yttrium at 50 GPa (filled squares connected with dashed line), and (b) hcp yttrium at 50 GPa (filled circles connected with solid line), and dhcp yttrium at ambient pressure (filled squares connected with dashed line). The solid and the dotted lines connecting the calculated points are only a guide to the eye.

function $\alpha^2 F(\omega)$ extends up to 41.8 meV in dhcp yttrium. The higher frequency couplings are more effective in raising the superconducting transition temperature than the lower frequency couplings.

The role played by the crystal structure in determining $F(\omega)$ and $\alpha^2 F(\omega)$ can be seen from Fig. 6 (b), where we show $F(\omega)$ and $\alpha^2 F(\omega)$ for the unstable hcp and dhcp yttrium phases. Not surprisingly, now it is the ambient pressure dhcp phase of yttrium which has a lower maximum frequency of 27.5 meV with the high pressure hcp phase having a higher maximum frequency of 43.6 meV. Consequently, the electron-phonon coupling is weaker in the dhcp phase than in the hcp phase, leading to $\lambda = 0.47$ for dhcp yttrium and $\lambda = 1.2$ for hcp yttrium.

To gain further insight into the nature of electron-phonon coupling, we show in Fig. 7 the \mathbf{q} -resolved partial $\lambda_{\mathbf{q}}$ along symmetry directions in the corresponding Brillouin zones for stable and unstable hcp and dhcp phases of yttrium. We find that as we go from ambient pressure hcp phase to high pressure dhcp phase, the electron-phonon coupling enhances substantially around symme-

Table II: The calculated average electron-phonon coupling constant λ , the root mean square frequency ω_{rms} and the superconducting transition temperature T_c obtained with $\mu^* = 0.2$, for yttrium as a function of structure and pressure. The T_c values given in the parentheses correspond to $\mu^* = 0.12$.

yttrium	pressure (GPa)	λ	ω_{rms} (K)	T_c (K)
hcp	0	0.55	193.5	0.3 (2.8)
hcp	50	1.21	221.7	15.9 (19.8)
dhcp	0	0.47	209.0	< 0.001(1.4)
dhcp	50	1.24	214.2	15.3 (19.0)

try points A and M, as can be seen from Fig. 7 (a). The contribution to λ from symmetry point A is $\lambda_{\mathbf{q}} = 8.1$, which arises from the lowest eight modes involving motion of all the four atoms in the $x-y$ plane. Similarly, at the symmetry point M, $\lambda_{\mathbf{q}} = 4.1$, with the lowest mode involving all the four atoms contributing around 1.6.

A comparison of $\lambda_{\mathbf{q}}$ for unstable dhcp and hcp phases with that of the stable hcp and dhcp phases shows significant contributions from symmetry point K, in addition to symmetry points A and M. The value of $\lambda_{\mathbf{q}} = 8.6$ at symmetry point A arises from the doubly degenerate, bond-stretching mode of the two basis atoms in the $x-y$ plane, each making a contribution of 3.8 to $\lambda_{\mathbf{q}}$.

We like to point out that the integrated values of $\lambda_{\mathbf{q}}$ for the unstable phases may be similar to the stable phases but the details are very different. We have also seen that a substantial contribution to $\alpha^2 F(\omega)$ and consequently to λ comes from a small region in reciprocal space, using a uniform grid to sample the space requires a dense grid of points. Thus, our calculated values of $\alpha^2 F(\omega)$ and consequently, λ can be improved upon by including more \mathbf{q} -points in the linear response calculations but it is unlikely to change the main conclusions of the present

work.

D. The Superconducting Transition Temperature

The possibility of superconductivity in hcp and dhcp yttrium within the present approach can be checked by solving numerically the isotropic gap equation^{16,17} using the calculated Eliashberg function $\alpha^2 F(\omega)$. The results of such a calculation for hcp and dhcp yttrium for two values of μ^* are shown in Table II. At ambient pressure, we find hcp yttrium to be superconducting with $T_c = 2.8$ K for $\mu^* = 0.12$ and $T_c = 0.3$ K for $\mu^* = 0.20$. In the high pressure dhcp phase, the T_c increases to 19.0 K for $\mu^* = 0.12$ and 15.3 K for $\mu^* = 0.20$, respectively. In Table II we have also listed the electron-phonon coupling constant λ , and the various averages of phonon frequencies for hcp and dhcp yttrium at both ambient and 50 GPa pressure.

IV. CONCLUSIONS

To understand the pressure-induced changes in electronic structure and electron-phonon interaction in yttrium, we have studied hexagonal close-packed (hcp) yttrium, stable at ambient pressure and double hexagonal close-packed (dhcp) yttrium, stable up to around 44 GPa, using density-functional-based methods. Our results show that as one goes from hcp yttrium to dhcp yttrium, there is (i) a substantial charge-transfer from $s \rightarrow d$ with extensive modifications of the d -band, (ii) a stiffening of phonon modes, (iii) an electron-phonon coupling over the entire extended frequency range with electron-phonon coupling constant λ changing from 0.55 to 1.24 and (iv) a change in the superconducting transition temperature T_c from 0.3 K to 15.3 K for $\mu^* = 0.2$, consistent with experiment.

* Electronic address: ppsingh@phy.iitb.ac.in

- ¹ C. Probst and J. Wittig, in *Handbook on the Physics and Chemistry of Rare Earths*, edited by J. K. A. Gschneidner and L. Eyring (North-Holland, Amsterdam, 1978), p. 749.
- ² J. J. Hamlin, V. G. Tissen, and J. S. Schilling, Phys. Rev. B **73**, 094522 (2006).
- ³ W. A. Grosshans and W. B. Holzapfel, Phys. Rev. B **45**, 5171 (1992).
- ⁴ Y. K. Vohra, H. Olijink, W. Grosshans, and W. P. Holzapfel, Phys. Rev. Lett. **47**, 1065 (1981).
- ⁵ K. Shimizu, H. Kimura, D. Takao, and K. Amaya, Nature **419**, 597 (2002).
- ⁶ V. V. Struzhkin, M. I. Erements, W. Gan, H.-K. Mao, and R. J. Hemely, Science **298**, 1213 (2002).
- ⁷ D. Kasinathan, J. Kunes, A. Lazicki, H. Rosner, C. S. Yoo, R. T. Scalettar, and W. E. Pickett, Phys. Rev. Lett. **96**, 047004 (2006).
- ⁸ G. Profeta, C. Franchini, N. N. Lathiotakis, A. Floris, A. Sanna, M. A. L. Marques, M. Luders, S. Massidda, E. K. U. Gross, and A. Continenza, Phys. Rev. Lett. **96**,

047004 (2006).

- ⁹ A. Sanna, C. Franchini, A. Floris, G. Profeta, N. N. Lathiotakis, M. Luders, M. A. L. Marques, E. K. U. Gross, A. Continenza, and S. Massidda, Phys. Rev. B **73**, 144512 (2006).
- ¹⁰ J. Melsen, J. M. Wills, B. Johansson, and O. Eriksson, Phys. Rev. B **48**, 15574 (1993).
- ¹¹ J. Wittig, Phys. Rev. Lett. **24**, 812 (1970).
- ¹² S. Y. Savrasov, Phys. Rev. B **54**, 16470 (1996).
- ¹³ S. Y. Savrasov and D. Y. Savrasov, Phys. Rev. B **54**, 16487 (1996).
- ¹⁴ *plane-wave self-consistent-field code*, <http://www.pwscf.org/>.
- ¹⁵ P. B. Allen and R. C. Dynes, Phys. Rev. B **12**, 905 (1975).
- ¹⁶ P. Allen and B. Mitrovic, in *Advances in Solid State Physics*, edited by H. Ehrenreich, F. Seitz, and E. Turnbull (Academic Press, New York, 1982), 37, p. 1.
- ¹⁷ P. B. Allen, private communication.
- ¹⁸ Z. P. Yin, S. Y. Savrasov, and W. E. Pickett, cond-mat/0606538.

- ¹⁹ J. P. Perdew and Y. Wang, Phys. Rev. B **45**, 13244 (1992).
- ²⁰ *xcrysden code*., <http://www.xcrysden.org/>.
- ²¹ F. Birch, Phys. Rev. **71**, 809 (1947).
- ²² S. J. Crowe, S. B. Dugdale, Z. Major, M. A. Alam, J. A. Duffy, and S. B. Palmer, Europhys. Lett. **65**, 235 (2004).
- ²³ R. Heid and K.-P. Bohnen, Phys. Rev. B **60**, R3709 (1999).